Sensor Fault Detection, Isolation, and Estimation in Lithium-Ion Batteries

Satadru Dey, Sara Mohon, Pierluigi Pisu, and Beshah Ayalew

***Abstract*— In battery management systems (BMSs), real-time diagnosis of sensor faults is critical for ensuring the safety and reliability of the battery. For example, a current sensor fault leads to erroneous estimates of state of charge and other parameters, which in turn affects the control actions in the BMS. A temperature sensor fault may lead to ineffective thermal management. In this brief, a model-based diagnostic scheme is presented that uses sliding mode observers designed based on the electrical and thermal dynamics of the battery. It is analytically shown how the extraction of the equivalent output error injection signals on the sliding manifolds enables the detection, the isolation, as well as the estimation of the temperature, voltage, and current sensor faults. This brief includes simulation and experimental studies to demonstrate and evaluate the effectiveness of the proposed scheme. Discussions are also included on the effects of uncertainty and on threshold design.**

***Index Terms*— Fault detection and isolation, fault estimation, Li-ion batteries, sensor fault, sliding mode observers.**

I. Introduction

ESTIMATION and control algorithms in battery management systems (BMSs) heavily depend on the real-time measurements of battery voltage, current, and temperature. Any fault in these sensors could hinder the BMS operation and lead to catastrophic scenarios. However, in the existing Li-ion battery literature, while several model-based state estimation algorithms are presented [1]–[4], the real-time fault diagnosis problem is much less explored.

The reviews of failure mechanisms and the diagnostics related challenges can be found in [5] and [6]. In [7], a nonlinear fault detection and isolation scheme has been developed to detect sensor and actuator faults. A Kalman-filter-based scheme was proposed in [8] to detect overcharge and overdischarge faults. A universal adaptive stabilization technique was proposed in [9] for diagnosing terminal voltage collapses. In [10], a set of Luenberger and learning observers were used for simultaneous fault isolation and estimation of a faulty cell in a battery string. In [11], diagnostic algorithms are presented for a battery pack. A fault detection and isolation strategy has been presented in [12] based on structural analysis.

Manuscript received February 2, 2016; accepted February 27, 2016. Manuscript received in final form February 29, 2016. The work of S. Dey was supported by the U.S. Department of Energy through the GATE Program under Grant DE-EE0005571. Recommended by Associate Editor S. Varigonda. *(Corresponding author: Satadru Dey.)*

S. Dey is with the Department of Civil and Environmental Engineering, University of California at Berkeley, Berkeley, CA 94720 USA (e-mail: satadru86@berkeley.edu).

S. Mohon, P. Pisu, and B. Ayalew are with the Clemson University-International Center for Automotive Research, Greenville, SC 29607 USA (e-mail: smohon@clemson.edu; pisup@clemson.edu; beshah@clemson.edu).

Color versions of one or more of the figures in this paper are available online at http://ieeexplore.ieee.org.

Digital Object Identifier 10.1109/TCST.2016.2538200

Most of these existing approaches detect and/or isolate some faults in the battery. However, very few of them actually *estimate* (some characteristics of) specific sensor faults. In this brief, we fill this gap and extend the aforementioned research by proposing a real-time diagnostic approach that detects, isolates, and estimates specific sensor faults, namely, the voltage, temperature, and current sensor faults. Note that completing the detection and isolation steps alone may indicate the fault occurrence and identify the faulty sensor, but sensor fault estimation can provide crucial added benefits for enhancing the reliability of BMSs. For example, current sensor fault information can help augment or correct the popular coulomb-counting-based state-of-charge (SOC) computation. Furthermore, current and temperature sensor fault information can help correct state-of-health parameter estimation schemes, which generally depend on SOC and temperature. Especially, in electric vehicle applications, it will enable the *limp-home mode* by allowing the vehicle to be driven safely to home or to a repair shop even after the occurrence of the fault. Broadly, sensor fault estimation can provide *fault-tolerance* capability to the BMS by allowing it to continue to function (although possibly in a degraded but safe mode) even after the sensor fault occurs.

In this brief, a diagnostic approach is presented that estimates the sensor faults along with their detection and isolation. As our focus is on output (sensor) faults, a model of the battery cell comprising of an equivalent electrical circuit coupled to a lumped thermal dynamics model is adopted for predicting the cell output behavior for its simple structure and low computational burden. The work adopts and builds on a sliding mode observer-based fault detection methodology presented in [13]. The basic idea to be exploited is that the *equivalent output error injection,* which is a continuous approximation (or filtered version) of the switching error injection term in the sliding mode observer, captures the fault information on the sliding surface. In this brief, three sliding mode observers are designed using the electrical plus thermal model. Then, on the sliding surfaces of each observer, a set of fault detection filter expressions are derived that are driven by the *equivalent output error injections* from the observers. The outputs of these filters are used as residual signals to detect, isolate, and estimate the sensor faults under the assumption that the faults and their time derivatives are bounded and finite. Analytical justifications of the proposed scheme are given using Lyapunov analysis for each fault scenario.

The rest of this brief is organized as follows. Section II briefly describes the battery cell model adopted for this work, and Section III briefs the diagnostics problem and outlines the detail design of the fault diagnosis scheme. Section IV presents discussions of some simulation and

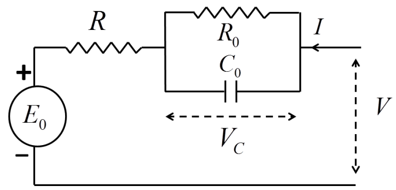

Fig. 1. Electrical equivalent circuit model.

experimental results. Section V summarizes the conclusion of this brief.

II. Lithium-Ion Cell Model

For a model of a battery cell, the commonly used equivalent electrical circuit (Fig. 1) plus the lumped thermal dynamics model are adopted.

The electrical dynamics of the battery cell can be written using Kirchoff's law, and with a usual definition of SOC

$$\dot{V}_c = -\frac{V_c}{R_0 C_0} + \frac{I}{C_0} \tag{1}$$

$$\dot{\mathrm{SOC}} = -\frac{I}{Q} \tag{2}$$

$$V = E_0 - IR - V_c \tag{3}$$

where V is the terminal voltage, I is the input current, R and R_0 and C_0 are the resistors and capacitors of the electrical circuit, respectively, V_c is the voltage across the capacitor C_0, E_0 is the open-circuit voltage, and Q is the charge capacity of the battery cell. The lumped thermal dynamics of the cell are given by

$$mc\dot{T} = I^2(R + R_0) - hA(T - T_{\mathrm{amb}}) \tag{4}$$

where T is the battery cell temperature, m is the mass, c is the specific heat capacity of the battery cell, hA is the effective heat transfer coefficient, and T_{amb} is the ambient temperature. Note that the open-circuit voltage is a function of SOC

$$E_0 = f(\mathrm{SOC}). \tag{5}$$

In the presence of sensor faults, the sensor outputs can be modeled by

$$I_{\mathrm{meas}} = I + \Delta_I, \quad V_{\mathrm{meas}} = V + \Delta_V, \quad T_{\mathrm{meas}} = T + \Delta_T \tag{6}$$

where I_{meas}, V_{meas}, and T_{meas} are the measured variables and Δ_I, Δ_V, and Δ_T are the current, voltage, and temperature sensor faults, respectively. It is assumed that Δ_k and $\dot{\Delta}_k$ are bounded by the finite values $|\Delta_k|_{\max}$ and $|\dot{\Delta}_k|_{\max}$, respectively, where $k \in \{I, V, T\}$. It is also assumed that no multiple faults can occur at the same time. Furthermore, we consider the case of small SOC ranges (valid for applications such as hybrid electric vehicles), where the parameters R, R_0, C_0, mc, and hA are constant and known with sufficient accuracy.

III. Diagnostic Problem and Proposed Scheme

In this brief, we mainly focus on the faults in the sensors: current sensor, voltage sensor, and temperature sensor. The impact of these faults in BMS operation is discussed in [12].

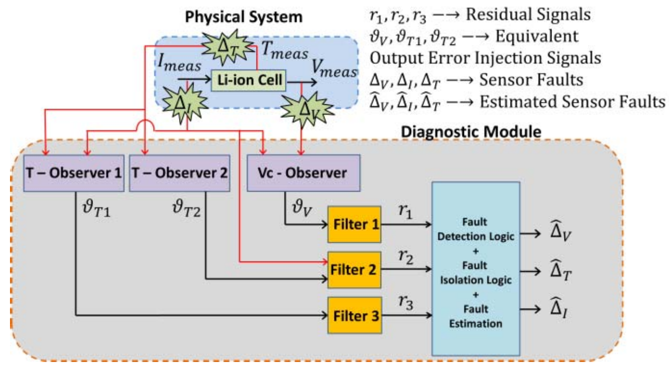

Fig. 2. Fault diagnosis scheme.

A. Diagnostic Scheme

The diagnostic scheme is shown in Fig. 2. In the following paragraphs, the elements of the scheme are described in detail.

1) *Observers:* In our scheme, we use three observers, one of which is based on (equivalent circuit) capacitor voltage V_c dynamics given in (1) [V_c-Observer in (7) and (8)] and the other two are based on temperature dynamics given in (4) [T-Observer 1 in (9) and T-Observer 2 in (10)]. From these observers, we extract the *equivalent output error injection* signals required to maintain the sliding motion [14].

a) *V_c-Observer:*

$$\dot{\widehat{V}}_c = -\frac{\widehat{V}_c}{R_0 C_0} + \frac{I_{\mathrm{meas}}}{C_0} + L_v \mathrm{sgn}(V_{c-\mathrm{meas}} - \widehat{V}_c) \tag{7}$$

$$V_{c-r} = E_0 - I_{\mathrm{meas}} R - V_{\mathrm{meas}} \tag{8}$$

where V_{c-r} is the reconstructed value of V_c, $L_v > 0$ is the tunable observer gain, and E_0 is calculated via $E_0 = f(\widehat{\mathrm{SOC}})$, where $\dot{\widehat{\mathrm{SOC}}} = -I_{\mathrm{meas}}/Q$ assuming Q is known with sufficient accuracy. Note that the initial SOC can be estimated from the $E_0 - \mathrm{SOC}$ map $f(\cdot)$ when the cell is at rest for a sufficient amount of time. However, some amount of SOC error and hence the E_0 error can be treated as uncertainties and suppressed by the nonzero thresholding scheme discussed in Section III-C.

b) *T-Observer 1:*

$$mc\dot{\widehat{T}}_1 = I_{\mathrm{meas}}^2(R + R_0) - hA(\widehat{T}_1 - T_{\mathrm{amb}}) + L_{T1}\mathrm{sgn}(T_{\mathrm{meas}} - \widehat{T}_1) \tag{9}$$

where $L_{T1} > 0$ is the tunable observer gain.

c) *T-Observer 2:*

$$mc\dot{\widehat{T}}_2 = -hA(\widehat{T}_2 - T_{\mathrm{amb}}) + L_{T2}\mathrm{sgn}(T_{\mathrm{meas}} - \widehat{T}_2) \tag{10}$$

where $L_{T2} > 0$ is the tunable observer gain.

2) *Filters:* Based on the error dynamics of V_c-Observer, T-Observer 1, and T-Observer 2 on the sliding surface, three filter expressions are derived. The outputs of these

filters are the residuals for fault detection, isolation, and estimation

$$\text{Filter 1: } \dot{r}_1 + \frac{r_1}{R_0C_0} = -\vartheta_V \tag{11}$$

where r_1 is the residual 1 and ϑ_V is the *equivalent output error injection* from V_c-Observer and essentially a continuous approximation (filtered version) of the switching signal $L_v\text{sgn}(V_{c-r} - \widehat{V}_c)$. The signal ϑ_V can be generated using the following equation: $\bar{\vartheta}_V(s) = G_V(s)U_V(s)$, where $\bar{\vartheta}_V(s)$ and $U_V(s)$ are the Laplace transforms of time-domain signals ϑ_V and $L_v\text{sgn}(V_{c-r} - \widehat{V}_c)$, respectively, and $G_V(s)$ is a user-defined low-pass filter

$$\text{Filter 2: } r_2 = |I_{\text{meas}}| - \sqrt{\vartheta_{T2}/(R+R_0)} \tag{12}$$

$$\text{Filter 3: } mc\dot{r}_3 + hAr_3 = \vartheta_{T1} \tag{13}$$

where r_2 and r_3 are the residuals 2 and 3, and ϑ_{T1} and ϑ_{T2} are the *equivalent output error injections* from T-Observer 1 and T-Observer 2, respectively. The signals ϑ_{T1} and ϑ_{T2} are continuous approximations (filtered versions) of the switching signals $L_{T1}\text{sgn}(T_{\text{meas}} - \widehat{T}_1)$ and $L_{T2}\text{sgn}(T_{\text{meas}} - \widehat{T}_2)$, respectively. The signals ϑ_{Ti} can be generated using the following equation: $\bar{\vartheta}_{Ti}(s) = G_{Ti}(s)U_{Ti}(s)$, where $\bar{\vartheta}_{Ti}(s)$ are the Laplace transforms of time-domain signals ϑ_{Ti}, $U_{Ti}(s)$ are the Laplace transforms of time-domain signals $L_{Ti}\text{sgn}(T_{\text{meas}} - \widehat{T}_i)$, and $G_{Ti}(s)$ are the user-defined low-pass filters (with $i = 1, 2$). Note that the low-pass filters $G_V(s)$ and $G_{Ti}(s)$ essentially extract the slow component of the actual switching signals and should have unity steady-state gains [13]. Next, we present the main result.

Proposition 1: Consider the system dynamics described by (1)–(5), the faulty sensor model described by (6), the observer structures (7)–(10), and the filter structures (11)–(13). If the observer gains satisfy the following conditions:

$$L_v > \max\{|f_1|_{\max}, |f_2|_{\max}\} > 0 \tag{14}$$

$$L_{T1} > \max\{|f_3|_{\max}, |f_4|_{\max}\} > 0 \tag{15}$$

$$L_{T2} > |f_5|_{\max} \geq |I|^2_{\max}(R+R_0) > 0 \tag{16}$$

where $|f_1|_{\max} = (|\tilde{V}_{c-\max}|/R_0C_0) + |\dot{\Delta}_V|_{\max}$, $|f_2|_{\max} = (|\tilde{V}_{c-\max}|/R_0C_0) + (|\Delta_I|_{\max}/C_0) + |\dot{\Delta}_{V2}|_{\max}$ with $\Delta_{V2} = \Delta E_0 - \Delta_I R$, where ΔE_0 is the result of SOC error due to the use of faulty current measurement, $|f_3|_{\max} = |\Delta_I|^2_{\max} + 2|\Delta_I|_{\max}|I|_{\max}(R+R_0)$, $|f_4|_{\max} = mc|\dot{\Delta}_T|_{\max} + hA|\Delta_T|_{\max}$, and $|f_5|_{\max} = mc|\dot{\Delta}_T|_{\max} + hA|\Delta_T|_{\max} + |I|^2_{\max}(R+R_0)$; then defining r_1, r_2, and r_3 as the residuals, the sensor faults can be detected and isolated by the fault signatures given in Table I.

Remark 1: As mentioned in Table I, the estimates of the voltage, current, and temperature sensor faults can be given by r_1, r_2, and r_3, respectively.

Proof: We analyze three sensor fault cases separately.

1) Case 1 (Occurrence of Voltage Sensor Fault Only): As the fault is only in the voltage sensor, $\Delta_V \neq 0$, whereas $\Delta_I = \Delta_T = 0$. Subtracting (7) from (1), the error dynamics of the $V_c -$ Observer can be written as

$$\dot{\tilde{V}}_c = -\frac{\tilde{V}_c}{R_0C_0} - L_v\text{sgn}(V_{c-r} - \widehat{V}_c) \tag{17}$$

with $\tilde{V}_c = V_c - \widehat{V}_c$ being the estimation error between the actual $V_c = (E_0 - IR - V)$ and the estimated $\widehat{V}_c$. Note that the sliding surface in this case is $s_V = V_{c-r} - \widehat{V}_c = \tilde{V}_c - \Delta_V$, which is inside the sign term. The reachability condition for this sliding surface can be analyzed by choosing a Lyapunov function candidate $W_1 = 0.5s_V^2$. Then

$$\dot{W}_1 = s_V\dot{s}_V = s_V(\dot{\tilde{V}}_c - \dot{\Delta}_V) \tag{18}$$

$$\Rightarrow \dot{W}_1 = s_V f_1 - L_v s_V \text{sgn}(s_V) \quad \text{with } f_1 = -\frac{\tilde{V}_c}{R_0C_0} - \dot{\Delta}_V. \tag{19}$$

Now applying the relationship $\bar{a}\bar{b} \leq |\bar{a}||\bar{b}|$ on the first term of the right-hand side of (19), we have

$$\dot{W}_1 \leq |s_V|(|f_1| - L_v). \tag{20}$$

Now, for a sufficiently high positive gain L_v, $\dot{W}_1 \leq 0$ and can be written as

$$\dot{W}_1 \leq -\alpha_1\sqrt{W_1} \quad \text{with } \alpha_1 = -\sqrt{2}(|f_1|_{\max} - L_v) > 0$$

$$\Rightarrow W_1(t) \leq \left\{-\frac{\alpha_1}{2}t + \sqrt{W_1(t_0)}\right\}^2. \tag{21}$$

Note that the observer gain should be selected such that it satisfies the condition $L_v > |f_1|_{\max} = (|\tilde{V}_{c-\max}|/R_0C_0) + |\dot{\Delta}_V|_{\max}$, where $|f_1|_{\max}$ will be bounded under the assumption that $|\dot{\Delta}_V|$ is bounded by a finite value $|\dot{\Delta}_V|_{\max}$. Further, $|\tilde{V}_{c-\max}|$ will be bounded if L_v is selected such that it suppresses the effect of $|\tilde{V}_c(t_0)|$, which is always bounded and thereafter $|\tilde{V}_c|$ will be nonincreasing $\forall t > t_0$. Therefore, it can be concluded that the sliding surface $s_V = 0$ will be achieved in some finite time $t_1 \leq 2\sqrt{W_1(t_0)}/\alpha_1$. On this sliding surface, we have $s_V = 0$ and $\dot{s}_V = 0$, which leads to

$$\tilde{V}_c - \Delta_V = 0 \tag{22}$$

$$\dot{\tilde{V}}_c - \dot{\Delta}_V = 0. \tag{23}$$

Now, using (17) and (22), (23) can be written as

$$\dot{\Delta}_V + \frac{\Delta_V}{R_0C_0} = -\vartheta_V \tag{24}$$

where ϑ_V is the *equivalent output error injection* signal defined after (11). As there is presence of fault Δ_V,

TABLE I

Fault Signature Table. 1 and 0 Denote Nonzero and Zero, Respectively

Residual Signals			Fault Detection/ Isolation	Fault Estimate Signal
r_1	r_2	r_3		
1	0	0	Voltage Sensor	r_1
0	1	1	Temperature Sensor	r_3
1	1	1	Current Sensor	r_2

the left-hand side of (24) will be nonzero, thereby making $\vartheta_V \neq 0$. Now comparing (11) and (24) and considering a zero initial condition for Δ_V and r_1, it can be concluded that $r_1 = \Delta_V$, which proves that r_1 is an estimate of the voltage sensor fault. A similar analysis can be performed for $T-$ Observer 1 and $T-$ Observer 2 using the Lyapunov function candidates $W_2 = 0.5mcs_{T1}^2$ and $W_3 = 0.5mcs_{T2}^2$, respectively, where $s_{Ti} = T_{\text{meas}} - \widehat{T}_i$ with $i = 1, 2$. In this case, the observers act under nominal conditions since faulty voltage measurement does not affect the thermal dynamics, and therefore, we have $r_2 = r_3 = 0$. The observer gains should satisfy the conditions $L_{T1} > 0$ and $L_{T2} > |I|_{\max}^2 (R + R_0)$ for error convergence.

2) Case 2 (Occurrence of Current Sensor Fault Only): In this case, we have only current sensor fault, and therefore, $\Delta_I \neq 0$, whereas $\Delta_V = \Delta_T = 0$. Subtracting (7) from (1), the error dynamics of the V_c- Observer can be written as

$$\dot{\tilde{V}}_c = -\frac{\tilde{V}_c}{R_0C_0} - \frac{\Delta_I}{C_0} - L_v\text{sgn}(V_{c-r} - \widehat{V}_c) \tag{25}$$

with $\tilde{V}_c = V_c - \widehat{V}_c$ being the estimation error between the actual $V_c = (E_0 - IR - V)$ and the estimated $\widehat{V}_c$. The sliding surface in this case is $s_V = V_{c-r} - \widehat{V}_c = E_0 + \Delta E_0 - (I+\Delta_I)R - V - \widehat{V}_c = \tilde{V}_c + \Delta E_0 - \Delta_I R$, which is inside the sign term. Note that the term ΔE_0 is the result of SOC computation error due to the use of faulty current measurement. Now, defining $\Delta E_0 - \Delta_I R = \Delta_{V2}$, the reachability condition for this sliding surface can be analyzed by choosing the Lyapunov function candidate $W_1 = 0.5s_V^2$. Then

$$\dot{W}_1 = s_V\dot{s}_V = s_V(\dot{\tilde{V}}_c + \dot{\Delta}_{V2}) \tag{26}$$

$$\Rightarrow \dot{W}_1 = s_V f_2 - L_v|s_V| \quad \text{with } f_2 = -\frac{\tilde{V}_c}{R_0C_0} - \frac{\Delta_I}{C_0} + \dot{\Delta}_{V2}. \tag{27}$$

Now applying $\bar{a}\bar{b} \leq |\bar{a}||\bar{b}|$ on the first term of the right-hand side of (27), we have

$$\dot{W}_1 \leq |s_V|(|f_2| - L_v). \tag{28}$$

If the gain L_v is sufficiently high and positive, $\dot{W}_1 \leq 0$ and can be written as

$$\dot{W}_1 \leq -\alpha_2\sqrt{W_1} \quad \text{with } \alpha_2 = -\sqrt{2}(|f_2|_{\max} - L_v) > 0$$
$$W_1(t) \leq \left\{-\frac{\alpha_2}{2}t + \sqrt{W_1(t_0)}\right\}^2. \tag{29}$$

Note that the observer gain should satisfy the condition $L_v > |f_2|_{\max} = (|\tilde{V}_{c-\max}|/R_0C_0) + (|\Delta_I|_{\max}/C_0) + |\dot{\Delta}_{V2}|_{\max}$, where $|f_2|_{\max}$ will be bounded under the assumption that $|\dot{\Delta}_{V2}|$ and $|\Delta_I|$ are bounded by the finite values $|\dot{\Delta}_{V2}|_{\max}$ and $|\Delta_I|_{\max}$, respectively. Therefore, it can be concluded from the above analysis that the sliding surface $s_V = 0$ will be achieved in some finite time $t_2 \leq 2\sqrt{W_1(t_0)}/\alpha_2$. On this sliding surface, we have $s_V = 0$ and $\dot{s}_V = 0$, which leads to

$$\tilde{V}_c + \Delta_{V2} = 0 \tag{30}$$
$$\dot{\tilde{V}}_c + \dot{\Delta}_{V2} = 0. \tag{31}$$

Now, using (25) and (30), (31) can be written as

$$\dot{\Delta}_{V2} + \frac{\Delta_{V2}}{R_0C_0} - \frac{\Delta_I}{C_0} = \vartheta_V \tag{32}$$

where ϑ_V is the *equivalent output error injection* signal defined after (11). Due to the presence of the fault Δ_I, the left-hand side of (32) will be nonzero, thereby making $\vartheta_V \neq 0$. As $\vartheta_V \neq 0$, it can be concluded that $r_1 \neq 0$ from (11).

Subtracting (9) from (4), the error dynamics of the $T-$ Observer 1 can be written as

$$mc\dot{\tilde{T}}_1 = \{I^2 - (I + \Delta_I)^2\}(R + R_0) - hA\tilde{T}_1$$
$$- L_{T1}\text{sgn}(T_{\text{meas}} - \widehat{T}_1) \tag{33}$$

with $\tilde{T}_1 = T - \widehat{T}_1$ being the estimation error between the actual T and the estimated $\widehat{T}_1$. Note that the sliding surface in this case is $s_{T1} = T_{\text{meas}} - \widehat{T}_1 = \tilde{T}_1$, which is inside the sign term. The reachability condition for this sliding surface can be analyzed by choosing the Lyapunov function candidate $W_2 = 0.5mcs_{T1}^2$. Then

$$\dot{W}_2 = s_{T1}\left(\left\{-\Delta_I^2 - 2\Delta_I I\right\}(R+R_0) - hAs_{T1} - L_{T1}\text{sgn}(s_{T1})\right). \tag{34}$$

Now applying $\bar{a}\bar{b} \leq |\bar{a}||\bar{b}|$ on the first term of the right-hand side of (34), we have

$$\dot{W}_2 \leq \left|-\Delta_I^2 - 2\Delta_I I\right|(R + R_0)|s_{T1}| - L_{T1}|s_{T1}|.$$

Now applying triangle inequality on the first term of the right-hand side of the above equation and then applying $\bar{a}\bar{b} \leq |\bar{a}||\bar{b}|$, we have

$$\dot{W}_2 \leq |f_3||s_{T1}| - L_{T1}|s_{T1}|$$
$$\text{with } |f_3| = |\Delta_I|^2 + 2|\Delta_I||I|(R + R_0).$$

For a sufficiently high choice of gain $L_{T1} > 0$, $\dot{W}_2 \leq 0$ and can be written as

$$\dot{W}_2 \leq -\alpha_3\sqrt{W_2}, \quad \alpha_3 = -\sqrt{2/mc}(|f_3|_{\max} - L_{T1}) > 0$$
$$\Rightarrow W_2(t) \leq \left\{-\frac{\alpha_3}{2}t + \sqrt{W_2(t_0)}\right\}^2. \tag{35}$$

Note that the observer gain should satisfy the condition $L_{T1} > |f_3|_{\max} = |\Delta_I|_{\max}^2 + 2|\Delta_I|_{\max}|I|_{\max}(R + R_0)$, where $|f_3|_{\max}$ will be bounded under the assumption that $I_{\max}$ is bounded and $|\Delta_I|$ is bounded by a finite value $|\Delta_I|_{\max}$. It can be concluded from (35) that the sliding surface $s_{T1} = 0$ will be achieved in some finite time $t_3 \leq 2\sqrt{W_2(t_0)}/\alpha_3$. On this sliding surface, we have $s_{T1} = \tilde{T}_1 = 0$ and $\dot{s}_{T1} = \dot{\tilde{T}}_1 = 0$. Under this condition, from (30), we can write $\vartheta_{T1} = \{I^2 - (I + \Delta_I)^2\}(R + R_0)$, where ϑ_{T1} is the *equivalent output error injection* signal defined after (13). Therefore, from (13), we can conclude that $r_3 \neq 0$.

For the error dynamics of the $T-$ Observer 2, a similar analysis can be performed using the Lyapunov function candidate $W_3 = 0.5mcs_{T2}^2$, where $s_{T2} = T_{\text{meas}} - \widehat{T}_2$. The observer gain should satisfy the condition $L_{T2} > |I|_{\max}^2(R+R_0)$ for the error convergence. Further, we can write $\vartheta_{T2} = I^2(R + R_0)$, where ϑ_{T2} is the *equivalent output error injection* signal defined after (13). However, in this case, we have $\Delta_I \neq 0$, and therefore, we can conclude from (12) that $r_2 \neq 0$.

Moreover, r_2 also estimates the amplitude of the fault. Note that the sign of the fault can be estimated by evaluating the sign of Δ_{V2} using the filter (32).

3) Case 3 (Occurrence of Temperature Sensor Fault Only): Here, we consider a temperature sensor fault leading to the condition $\Delta_T \neq 0$, whereas $\Delta_I = \Delta_V = 0$. In this case, the V_c − Observer acts under nominal conditions since faulty temperature measurement does not affect the voltage error dynamics, and therefore, we have $r_1 = 0$. The observer gain should satisfy the condition $L_v > 0$ for nominal error convergence. Subtracting (9) from (4), the error dynamics of the T − Observer 1 can be written as

$$mc\dot{\tilde{T}}_1 = -hA\tilde{T}_1 - L_{T1}\mathrm{sgn}(T_{\mathrm{meas}} - \widehat{T}_1) \quad (36)$$

with $\tilde{T}_1 = T - \widehat{T}_1$ being the estimation error between the actual T and the estimated $\widehat{T}_1$. Note that the sliding surface in this case is $s_{T1} = T_{\mathrm{meas}} - \widehat{T}_1 = \tilde{T}_1 + \Delta_T$, which is inside the sign term. The reachability condition for this sliding surface can be analyzed by choosing a Lyapunov function candidate $W_2 = 0.5mcs_{T1}^2$. Then

$$\dot{W}_2 = s_{T1}(mc\dot{\Delta}_T - hAs_{T1} + hA\Delta_T - L_{T1}\mathrm{sgn}(s_{T1})) \quad (37)$$

$$\Rightarrow \dot{W}_2 \leq (|f_4| - L_{T1})|s_{T1}| \quad \text{with} \quad f_4 = mc\dot{\Delta}_T + hA\Delta_T. \quad (38)$$

Now, for a sufficiently high positive gain L_{T1}, $\dot{W}_2 \leq 0$ and can be written as

$$\dot{W}_2 \leq -\alpha_4\sqrt{W_2}, \quad \text{with } \alpha_4 = -\sqrt{2/mc}(|f_4|_{\max} - L_{T1}) > 0$$
$$\Rightarrow W_2(t) \leq \left\{-\frac{\alpha_4}{2}t + \sqrt{W_2(t_0)}\right\}^2. \quad (39)$$

Note that the observer gain should satisfy the condition $L_{T1} > |f_4|_{\max} = mc|\dot{\Delta}_T|_{\max} + hA|\Delta_T x|_{\max}$, where $|f_4|_{\max}$ will be bounded under the assumption that Δ_T and $\dot{\Delta}_T$ are bounded by the finite values $|\Delta_T|_{\max}$ and $|\dot{\Delta}_T|_{\max}$. Therefore, from the above analysis, it can be concluded that the sliding surface $s_{T1} = 0$ will be achieved in some finite time $t_4 \leq 2\sqrt{W_2(t_0)}/\alpha_4$. In this sliding surface, we have $s_{T1} = \tilde{T}_1 + \Delta_T = 0$ and $\dot{s}_{T1} = \dot{\tilde{T}}_1 + \dot{\Delta}_T = 0$. Under this condition, from (36), we can write that

$$mc\dot{\Delta}_T + hA\Delta_T = \vartheta_{T1} \quad (40)$$

where ϑ_{T1} is the *equivalent output error injection* signal defined after (13). As there is presence of fault Δ_T, the left-hand side of (40) will be nonzero, thereby making $\vartheta_{T1} \neq 0$.

Now comparing (13) and (40), it can be concluded that $r_3 = \Delta_T$, which proves that r_3 is an estimate of the temperature sensor fault.

Subtracting (10) from (4), the error dynamics of the T − Observer 2 can be written as

$$mc\dot{\tilde{T}}_2 = I^2(R + R_0) - hA\tilde{T}_2 - L_{T2}\mathrm{sgn}(T_{\mathrm{meas}} - \widehat{T}_2) \quad (41)$$

with $\tilde{T}_2 = T - \widehat{T}_2$ being the estimation error between the actual T and the estimated $\widehat{T}_2$. Note that the sliding surface in this case is $s_{T2} = T_{\mathrm{meas}} - \widehat{T}_2 = \tilde{T}_2 + \Delta_T$, which is inside the sign term. The reachability condition for this sliding surface can be analyzed by choosing a Lyapunov function candidate $W_3 = 0.5mcs_{T2}^2$. Then

$$\dot{W}_3 = s_{T2}\{I^2(R + R_0) + mc\dot{\Delta}_T + hA\Delta_T - hAs_{T2} - L_{T2}\mathrm{sgn}(s_{T2})\} \quad (42)$$

$$\Rightarrow \dot{W}_3 \leq (|f_5| - L_{T2})|s_{T2}|$$
$$\text{with } f_5 = I^2(R + R_0) + mc\dot{\Delta}_T + hA\Delta_T. \quad (43)$$

Now, for a sufficiently high positive gain L_{T2}, $\dot{W}_3 \leq 0$ and can be written as

$$\dot{W}_3 \leq -\alpha_5\sqrt{W_3}, \quad \alpha_5 = -\sqrt{2/mc}(|f_5|_{\max} - L_{T2})$$
$$\Rightarrow W_3(t) \leq \left\{-\frac{\alpha_5}{2}t + \sqrt{W_3(t_0)}\right\}^2. \quad (44)$$

Note that the observer gain should satisfy the condition $L_{T2} > |f_5|_{\max} = mc|\dot{\Delta}_T|_{\max} + hA|\Delta_T|_{\max} + |I|_{\max}^2(R + R_0)$, where $|f_5|_{\max}$ will be bounded under the assumption that Δ_T, $\dot{\Delta}_T$ and I are bounded, respectively, by the finite values $|\Delta_T|_{\max}$, $|\dot{\Delta}_T|_{\max}$, and $|I|_{\max}$. Therefore, from the above analysis, it can be concluded that the sliding surface $s_{T2} = 0$ will be achieved in some finite time $t_5 \leq 2\sqrt{W_3(t_0)}/\alpha_5$. In this sliding surface, we have $s_{T2} = \tilde{T}_2 + \Delta_T = 0$ and $\dot{s}_{T2} = \dot{\tilde{T}}_2 + \dot{\Delta}_T = 0$. Under this condition, from (41), we can write $\vartheta_{T2} = mc\dot{\Delta}_T + hA\Delta_T + I^2(R + R_0)$, where ϑ_{T2} is the *equivalent output error injection* signal defined after (13). Therefore, from (12), we can conclude that $r_2 \neq 0$. □

B. Effect of Modeling, Parametric, and Measurement Uncertainties

Although the battery system parameters are assumed to be constant at the design phase, in reality, they may vary due to temperature and current dependencies. Furthermore, there will be measurement and modeling uncertainties. In this section, we will analyze uncertainties affecting the proposed diagnostic scheme. With the inclusion of the additive uncertainties, the V_c dynamics (1) and the output (8) can be rewritten as

$$\dot{V}_c = -\frac{V_c}{R_0C_0} + \frac{I}{C_0} + \eta_1 \quad (45)$$
$$V_{c-r} = E_0 - I_{\mathrm{meas}}R - V_{\mathrm{meas}} + \eta_2 \quad (46)$$

where η_1 and η_2 are the lumped effects of the uncertainties, which can be nonlinear functions of states and inputs, respectively. We assume that uncertainties and their derivatives are bounded, i.e., $\eta_2, \eta_1, \dot{\eta}_1, \dot{\eta}_2 \in L_\infty$. Now, in the presence of no sensor faults, the error dynamics of the V_c − Observer can be rewritten as

$$\dot{\tilde{V}}_c = -\frac{\tilde{V}_c}{R_0C_0} - L_v\mathrm{sgn}(\tilde{V}_c + \eta_2) + \eta_1. \quad (47)$$

Note that the sliding surface here is $s_V = \tilde{V}_c + \eta_2$. Now, even in the absence of any faults, the *equivalent output error injection* signal $\vartheta_V \neq 0$ due to the presence of uncertainties. However, ϑ_V will be bounded with the assumption of $\eta_2, \eta_1, \dot{\eta}_2 \in L_\infty$. The signal ϑ_V and therefore the residual r_1 will be nonzero even if there is no fault. Under these uncertainties, an upper bound on the residual r_1 can be computed as follows.

This article has been accepted for inclusion in a future issue of this journal. Content is final as presented, with the exception of pagination.

We assume that the observer gain $L_v > 0$ is sufficiently high to have reachability to the sliding surface. At the sliding surface, we have $s_V = 0$ and $\dot{s}_V = 0$, which leads to: $\tilde{V}_c + \eta_2 = 0$ and $\dot{\tilde{V}}_c + \dot{\eta}_2 = 0$. Therefore, (47) can be written as

$$\vartheta_V = \dot{\eta}_2 + \frac{\eta_2}{R_0 C_0} + \eta_1. \tag{48}$$

Substituting the above expression for ϑ_V in (11)

$$\dot{r}_1 + \frac{r_1}{R_0 C_0} = -\dot{\eta}_2 - \frac{\eta_2}{R_0 C_0} - \eta_1 \tag{49}$$

$$\Rightarrow \frac{d(r_1 + \eta_2)}{dt} + \frac{(r_1 + \eta_2)}{R_0 C_0} = -\eta_1. \tag{50}$$

From the solution of differential equation (50) and denoting $\alpha = 1/R_0 C_0$, the time evolution of the signal $(r_1 + \eta_2)$ can be written as

$$r_1(t) = -\eta_2(t) + \{r_1(0) + \eta_2(0)\}e^{-\alpha t} - \int_0^t e^{-\alpha(t-\tau)}\eta_1(\tau)d\tau.$$

Using triangle inequality, the relationship $\bar{a}\bar{b} \leq |\bar{a}||\bar{b}|$, the uncertainty bounds $|\eta_i| \leq |\eta_i|_{\max}$ and $|\dot{\eta}_i| \leq |\dot{\eta}_i|_{\max}$ with $i \in \{1, 2\}$, and the fact that $e^{-\alpha t} > 0$, $\forall t \geq 0$, implies $|e^{-\alpha t}| = e^{-\alpha t}$, $\forall t \geq 0$, the upper bound of r_1 can be derived as

$$|r_1(t)| \leq |\eta_2|_{\max} + \{|r_1(0)| + |\eta_2|_{\max}\}e^{-\alpha t} + \int_0^t e^{-\alpha(t-\tau)}|\eta_1|_{\max} d\tau. \tag{51}$$

Therefore, it can be concluded that the estimate of the voltage sensor fault using (11) will be corrupted by the effect of uncertainties.

C. Threshold Design for Residuals: Passive Robustness to Uncertainties

To suppress the effect of uncertainties, we design some nonzero constant threshold values against which the residuals will be compared. The residual evaluation logic will be as follows: residual $\geq$ threshold indicates fault and residual $<$ threshold indicates no fault. To design the threshold, we collect residual data under nonfaulty conditions either by Monte Carlo simulation or experimental studies. Then, we plot the probability distribution of the residuals. One example probability distribution is shown in Fig. 3. Note that this particular example probability distribution is generated based on the assumption of zero-mean Gaussian distribution of the uncertainties. In reality, this probability distribution will depend on uncertainties in the experimental data or of the Monte Carlo study. Then, we select a maximum allowable probability of false alarms.

From Fig. 3, it can be seen that the probability of the false alarms can be computed by the following equation:

$$P_{\mathrm{FA}} = \int_{-\infty}^{-\mathrm{th}} p_0(x)dx + \int_{\mathrm{th}}^{+\infty} p_0(x)dx \tag{52}$$

where th is the selected threshold and p_0 is the residual's probability distribution under no fault. The goal here is to select th, which will give the acceptable P_{FA} from (52).

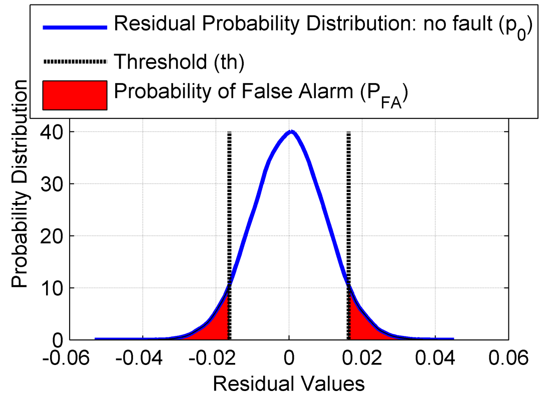

Fig. 3. Residual probability distribution under no fault.

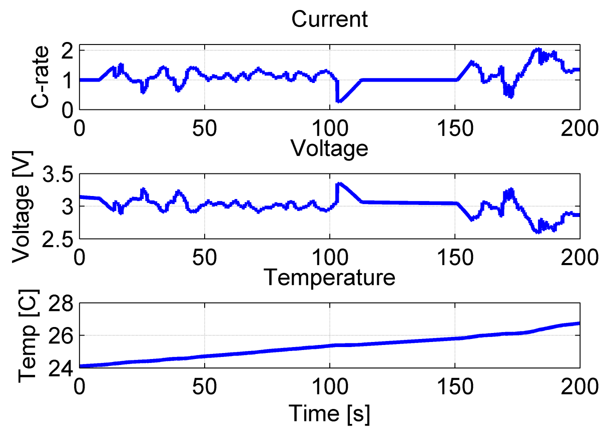

Fig. 4. Dynamic discharge current profile and corresponding voltage and temperature responses (model outputs) under no fault condition.

IV. Simulation and Experimental Results

In this section, we test the effectiveness of the proposed diagnostic scheme by conducting simulation and experimental studies on a commercial A123 Li-ion battery cell. The studies are conducted on a constant parameter scenario, as discussed in Section III-A. First, using the experimental data, battery model parameters are extracted by fitting the battery model to the experimental data. This is done by solving an optimization problem, where a set of parameters that minimize the difference between experimental and model simulated data were identified. The identified model parameters are $R = 0.2$, $R_0 = 0.019$, $C_0 = 600$, $mc = 180$, $hA = 0.4$, and $E_0 = 2.939 + 0.01939 * \mathrm{SOC} - 0.000377 * \mathrm{SOC}^2 + 2.452 \times 10^{-6} * \mathrm{SOC}^3$.

A. Simulation Studies

Now, using the battery model identified in the previous step, we first perform simulation studies. To emulate a realistic scenario, measurement noise has been injected to the sensor outputs (standard deviation: 80-mA current noise, 50-mV voltage noise, and 0.5 °C temperature noise). To generate thresholds, the probability distribution of the nonfaulty residuals has been generated by a Monte Carlo study with 5% acceptable false alarm probability. For a cell-level diagnostic

This article has been accepted for inclusion in a future issue of this journal. Content is final as presented, with the exception of pagination.

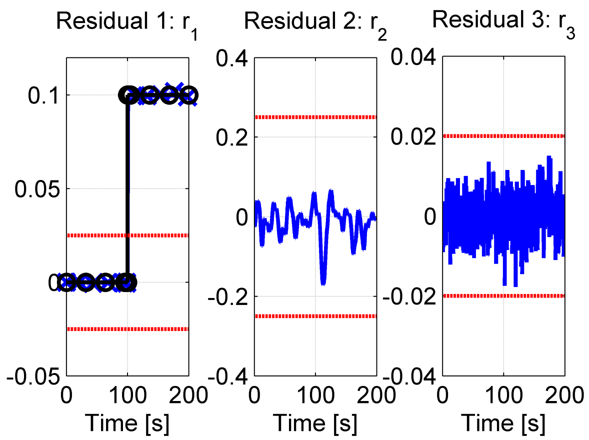

Fig. 5. Residual responses for a voltage sensor bias fault of 0.1 V (injected at 100 s). The solid blue line represents the residuals and the red line represents the thresholds. Leftmost: the solid black line represents the injected fault and the blue line with x markers represents the $\boldsymbol{r_1}$ residual.

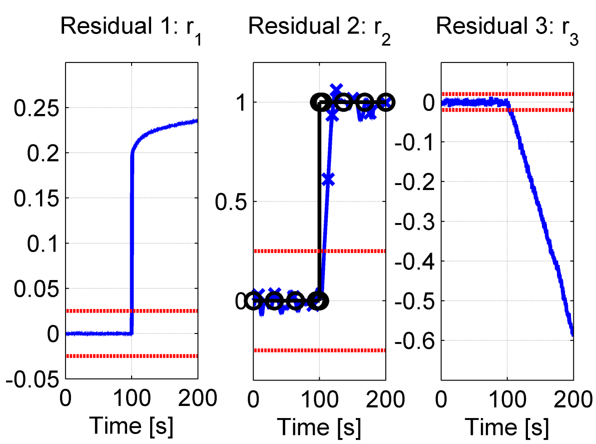

Fig. 6. Residual responses for a current sensor bias fault of 1 A (injected at 100 s). The solid blue line represents the residuals and the red line represents the thresholds. Middle: the solid black line represents the injected fault and the blue line represents the $\boldsymbol{r_2}$ residual.

study, a modified Urban Dynamometer Driving Schedule-like dynamic discharge current profile has been used as shown in Fig. 4 along with the corresponding voltage and temperature response.

Bias-type faults were injected to evaluate the performance of the scheme. The results are given in Figs. 5–7 for a voltage sensor bias fault of 0.1 V, a current sensor bias fault of 1 A, and a temperature sensor bias fault of 1 °C, respectively. Note that the diagnostic scheme is able to detect, isolate, and estimate the faults as per the fault signatures in Table I.

Next, we evaluate the performance of the diagnostic scheme in the presence of the parametric uncertainties. To this end, we examine the fault estimation errors and false alarm rates in such conditions. In the plant model, several important parameters (R, R_0, C_0, hA, and Q) are deviated from their nominal values to induce the uncertainties. The parameter deviations and corresponding estimation errors and false alarm rates are shown in Table II. It can be noted that the scheme significantly degrades under the deviation in the parameter R,

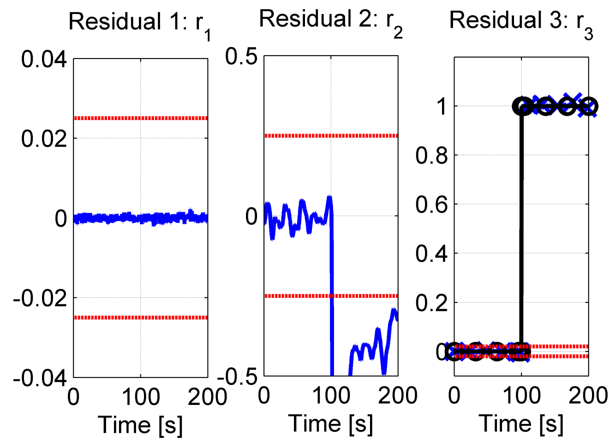

Fig. 7. Residual responses for a temperature sensor bias fault of 1 °C (injected at 100 s). The solid blue line represents the residuals and the red line represents the thresholds. Rightmost: the solid black line represents the injected fault and the blue line with x markers represents the $\boldsymbol{r_3}$ residual.

TABLE II
EFFECT OF PARAMETRIC UNCERTAINTIES

Parametric Uncertainties	%Error in Δ_V estimation	%Error in Δ_I estimation	%Error in Δ_T estimation	False Alarm Rate
20% variation in R	80%	30%	10%	High
20% variation in R_0	10%	1%	2%	Low
20% variation in C_0	1%	<1%	<1%	Low
20% variation in hA	<1%	10%	5%	Low
20% variation in Q	10%	<1%	<1%	Low

as evident in the large estimation errors and high false alarm rates. This is reasonable because the parameter R represents a large part of the battery internal resistance and hence is the most sensitive part of the electrical and thermal dynamics. Other than R, the performance of the scheme is acceptable under the given deviations in the rest of the parameters.

B. Experimental Studies

In this brief, we show the effectiveness of the proposed scheme using experimental data collected from the physical battery. The experimental data along with the model data are shown in Fig. 8. To generate thresholds, the probability distribution of the nonfaulty residuals has been generated under different operating conditions by varying the input current up to 5C and different initial temperature conditions in 15 °C–40 °C range with 5% acceptable false alarm probability. Current profiles used in the study are constant discharge currents of 1C, 3C, and 5C and pulse discharge currents with pulse amplitudes of 1C and 4C. In the experimental data, we injected constant bias faults in the battery sensor outputs. The results given in Figs. 9–11 for a voltage sensor bias fault of 0.5 V, a current sensor fault of 2 A, and a temperature sensor bias fault of 2 °C, respectively, show a reasonable performance for the scheme. Note that in Fig. 11, the residual r_2 goes below the threshold toward the end. This is because the presence of uncertainty attenuates the fault effect in the residual. However, this should not affect the diagnosis as the residual was high

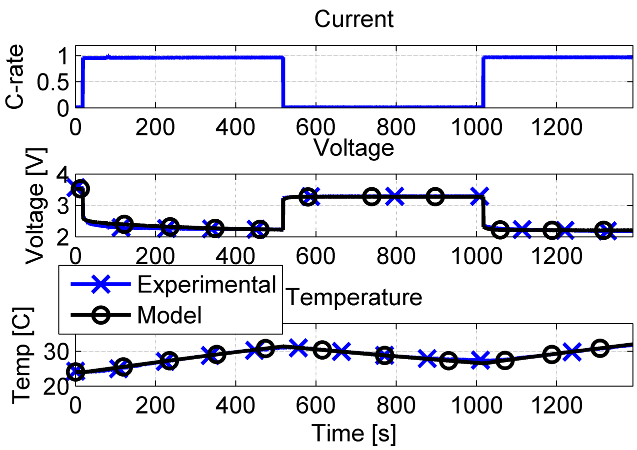

Fig. 8. Current profile and corresponding voltage and temperature responses measured from the battery under no fault condition. The experimental voltage and temperature are compared with model outputs.

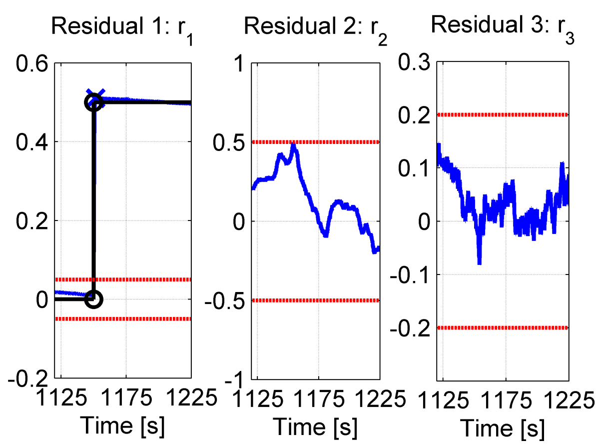

Fig. 9. Residual responses for a voltage sensor bias fault of 0.5 V (injected at 1150 s). The solid blue line represents the residuals and the red line represents the thresholds. Leftmost: the solid black line represents the injected fault and the blue line with x markers represents the $\boldsymbol{r_1}$ residual.

for a long period of time. To mitigate such effects, one might include the residual *up time* in the scheme to infer the presence of faults.

It can be seen that while the detection and isolation are successful, the estimates of the bias faults include errors due to uncertainties. In this study, we have found that the current, voltage, and temperature sensor fault estimation errors are within 3%, 10%, and 5%, respectively. Note that the filters (11)–(13) that are generating the residuals are stable. Therefore, as long as the uncertainties and their derivatives remain bounded, the fault estimates will be bounded around the neighborhood of the actual fault.

In the case of structured uncertainties that are far different from the fault in their frequency domain characteristics, it is possible to decouple the fault information from the uncertainties via appropriate filtering mechanisms. However, it is observed that in the case of batteries, the uncertainties are unstructured and can be close to or overlap with the frequency domain characteristics of the faults, which makes it very difficult to suppress their effects completely.

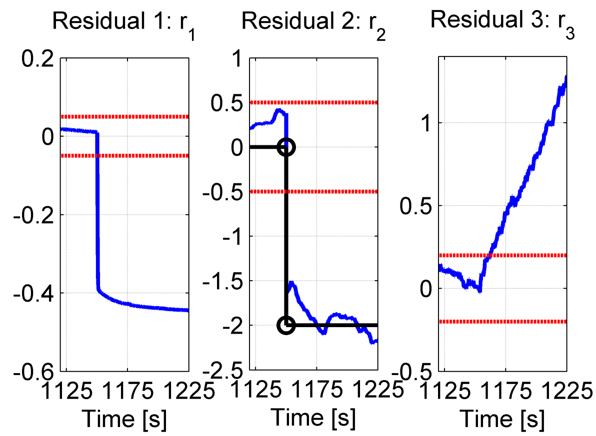

Fig. 10. Residual responses for current sensor bias fault of 2 A (injected at 1150 s). The solid blue line represents the residuals and the red line represents the thresholds. Middle: the solid black line represents the injected fault and the blue line represents the $\boldsymbol{r_2}$ residual.

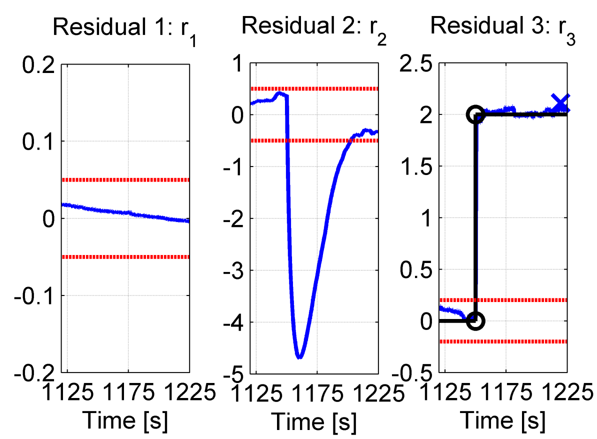

Fig. 11. Residual responses for temperature sensor bias fault of 2 °C (injected at 1150 s). The solid blue line represents the residuals and the red line represents the thresholds. Rightmost: the solid black line represents the injected fault and the blue line with x markers represents the $\mathbf{r_3}$ residual.

V. Conclusion

This brief outlined a diagnostic scheme for detecting, isolating, and estimating sensor faults in Li-ion batteries. The scheme uses three sliding mode observers based on the electrical and thermal dynamics of the battery. Further, some filter expressions have been derived using dynamics at the sliding motion, which are driven by the *equivalent output injection errors* from the sliding mode observers. The effect of modeling and parametric uncertainties on the diagnostic scheme has been analyzed. Finally, simulation and experimental studies have been conducted in a commercial A123 Li-ion battery cell to demonstrate the potential of the approach.

References

[1] S. J. Moura, N. A. Chaturvedi, and M. Krstić, "PDE estimation techniques for advanced battery management systems—Part I: SOC estimation," in *Proc. Amer. Control Conf.*, Jun. 2012, pp. 559–565.

[2] G. L. Plett, "Extended Kalman filtering for battery management systems of LiPB-based HEV battery packs: Part 3. State and parameter estimation," *J. Power Sour.*, vol. 134, no. 2, pp. 277–292, 2004.

[3] S. Dey, B. Ayalew, and P. Pisu, "Nonlinear robust observers for state-of-charge estimation of lithium-ion cells based on a reduced electrochemical model," *IEEE Trans. Control Syst. Technol.*, vol. 23, no. 5, pp. 1935–1942, Sep. 2015.

[4] S. Dey, B. Ayalew, and P. Pisu, "Nonlinear adaptive observer for a lithium-ion battery cell based on coupled electrochemical–thermal model," *ASME J. Dyn. Syst., Meas. Control*, vol. 137, no. 11, p. 111005, Aug. 2015.

[5] D. Aurbach, E. Zinigrad, Y. Cohen, and H. Teller, "A short review of failure mechanisms of lithium metal and lithiated graphite anodes in liquid electrolyte solutions," *Solid State Ionics*, vol. 148, pp. 405–416, Jun. 2002.

[6] S. M. M. Alavi, M. F. Samadi, and M. Saif, "Diagnostics in lithium-ion batteries: Challenging issues and recent achievements," in *Integration of Practice-Oriented Knowledge Technology: Trends and Prospectives*. Heidelberg, Germany: Springer, 2013, pp. 277–291.

[7] J. Marcicki, S. Onori, and G. Rizzoni, "Nonlinear fault detection and isolation for a lithium-ion battery management system," in *Proc. ASME Dyn. Syst. Control Conf.*, 2010, pp. 607–614.

[8] A. Singh, A. Izadian, and S. Anwar, "Fault diagnosis of Li-ion batteries using multiple-model adaptive estimation," in *Proc. 39th Annu. Conf. IEEE IECON*, Nov. 2013, pp. 3524–3529.

[9] S. Mukhopadhyay and F. Zhang, "Adaptive detection of terminal voltage collapses for Li-ion batteries," in *Proc. IEEE 51st Annu. Conf. Decision Control*, Dec. 2012, pp. 4799–4804.

[10] W. Chen, W.-T. Chen, M. Saif, M.-F. Li, and H. Wu, "Simultaneous fault isolation and estimation of lithium-ion batteries via synthesized design of Luenberger and learning observers," *IEEE Trans. Control Syst. Technol.*, vol. 22, no. 1, pp. 290–298, Jan. 2014.

[11] W. Lombardi, M. Zarudniev, S. Lesecq, and S. Bacquet, "Sensors fault diagnosis for a BMS," in *Proc. Eur. Control Conf.*, Jun. 2014, pp. 952–957.

[12] Z. Liu, Q. Ahmed, G. Rizzoni, and H. He, "Fault detection and isolation for lithium-ion battery system using structural analysis and sequential residual generation," in *Proc. ASME Dyn. Syst. Control Conf.*, 2014, p. V002T36A005.

[13] C. Edwards, S. K. Spurgeon, and R. J. Patton, "Sliding mode observers for fault detection and isolation," *Automatica*, vol. 36, no. 4, pp. 541–553, 2000.

[14] V. Utkin, J. Guldner, and J. Shi, *Sliding Mode Control in Electro-Mechanical Systems*. Boca Raton, FL, USA: CRC Press, 1999.